

# Tunable Magnetically Induced Transparency Spectra in Magnon-Magnon Coupled $\text{Y}_3\text{Fe}_5\text{O}_{12}$ /Permalloy Bilayers

Yuzan Xiong,<sup>1,2,3</sup> Jerad Inman,<sup>1,2</sup> Zhengyi Li,<sup>4</sup> Kaile Xie,<sup>4</sup> Rao Bidthanapally,<sup>1</sup> Joseph Sklenar,<sup>5</sup> Peng Li,<sup>6</sup> Steven Louis<sup>6</sup>,<sup>2</sup> Vasyl Tyberkevych,<sup>1</sup> Hongwei Qu,<sup>2</sup> Zhili Xiao,<sup>3</sup> Wai K. Kwok<sup>6</sup>,<sup>3</sup> Valentine Novosad,<sup>3</sup> Yi Li,<sup>3,\*</sup> Fusheng Ma<sup>4,†</sup>, and Wei Zhang<sup>6,‡</sup>

<sup>1</sup>*Department of Physics, Oakland University, Rochester, Michigan 48309, USA*

<sup>2</sup>*Department of Electronic and Computer Engineering, Oakland University, Rochester, Michigan 48309, USA*

<sup>3</sup>*Materials Science Division, Argonne National Laboratory, Argonne, Illinois 60439, USA*

<sup>4</sup>*Jiangsu Key Laboratory of Opto-Electronic Technology, School of Physics and Technology, Nanjing Normal University, Nanjing 210046, China*

<sup>5</sup>*Department of Physics and Astronomy, Wayne State University, Detroit, Michigan 48201, USA*

<sup>6</sup>*Department of Electrical and Computer Engineering, Auburn University, Auburn, Alabama 36849, USA*



(Received 18 November 2021; revised 22 January 2022; accepted 11 March 2022; published 6 April 2022)

Hybrid magnonic systems host a variety of characteristic phenomena such as the magnetically induced transparency (MIT) and Purcell effect, which are considered useful for future coherent quantum-information processing. In this work, we experimentally demonstrate a tunable MIT effect in the  $\text{Y}_3\text{Fe}_5\text{O}_{12}$ (YIG)/Permalloy(Py) magnon-magnon coupled system via changing the magnetic field orientations. By probing the magneto-optic effects of Py and YIG thin films, we identify clear features of MIT spectra induced by the mode hybridization between the uniform mode of Py and the perpendicular standing spin-wave modes of YIG. By changing the external magnetic field orientations, we observe a tunable coupling strength between the YIG's spin-wave modes and the Py's uniform mode, upon the application of an out-of-plane magnetic field. This observation is theoretically interpreted by a geometrical consideration of the Py and YIG magnetization under the oblique magnetic field even at a constant interfacial exchange coupling. Our findings show high promise for investigating tunable coherent phenomena with hybrid magnonic platforms.

DOI: [10.1103/PhysRevApplied.17.044010](https://doi.org/10.1103/PhysRevApplied.17.044010)

## I. INTRODUCTION

Hybrid magnonic systems are rising contenders for coherent information processing, owing to their capability of coherently connecting distinct physical platforms in quantum systems and their rich emerging quantum-engineering functionalities [1–5]. Recent studies have revealed strong, coherent hybridization of magnons with phonons, microwave photons, and optical light, with the observation of characteristic phenomena such as the strong and ultrastrong coupling, magnetically induced transparency (MIT), and Purcell effect [6–13]. In addition, to fully leverage the hybrid coupling phenomena with magnons, strong and tunable couplings between two magnonic systems have recently attracted considerable attention [14–18]. These systems can be considered as hosting hybrid magnonic modes in a “magnonic cavity,”

analogous to the microwave photonic cavity in cavity-magnon polaritons.

So far, studies of magnon-magnon coupling have been largely centered around the strong coupling regime, with a characteristic observation of the anticrossing gap between the two intersecting magnonic modes. In such a strong coupling regime, the coupling strength,  $g/2\pi$ , is greater than the dissipation rate of both coupling entities,  $\kappa_a/2\pi$ ,  $\kappa_b/2\pi$ , as illustrated in Fig. 1(a). On the other hand, the regime where  $g/2\pi$  is weaker than both dissipation rates is known as the weak coupling. In between the strong and weak coupling regimes, the coupling satisfies  $\kappa_b < g < \kappa_a$ , and two characteristic quantum phenomena can be observed, namely, the MIT and Purcell effects [12], depending on which magnon resonator is to be pumped. The MIT effect is the magnetic analogy of electromagnetically induced transparency (EIT). One example is a spin-wave-induced suppression of the ferromagnetic resonance (FMR) of another adjacent layer [19,20]. The Purcell effect is characterized with an enhanced decay of the cavity photon due to its coupling

\*yili@anl.gov

†phymafs@njnu.edu.cn

‡weizhang@oakland.edu

to lossy magnons. In conventional magnon-photon coupled systems, the two effects are, respectively, discussed with the magnon and the photon subsystems. In magnon-magnon coupled systems, the two effects are reciprocal, i.e., the MIT effect of  $m_a$  is simultaneously accompanied with the Purcell effect of  $m_b$ , as illustrated in Fig. 1(b). Such an MIT effect in magnon-magnon coupled systems was earlier reported in  $\text{Y}_3\text{Fe}_5\text{O}_{12}$ (YIG)/Permalloy(Py) thin-film bilayers, by probing the coupled magnetization dynamics via the magneto-optic Kerr and Faraday effects [17].

## II. SAMPLE AND MEASUREMENT

In this work, we further examine the magnetic field tunability of the magnon-magnon coupled mode spectra in the MIT regime. We probe the resonant magneto-optical signals of YIG/Py bilayers under two different magnetic-field-varying configurations, i.e., out-of-plane (OOP)  $\phi$  and in-plane (IP)  $\theta$  rotating-field geometries. In addition, our measurement setup allows us to optionally introduce a static OOP field by a permanent magnet when the magnetic field is swept in plane. A detailed depiction of the measurement construction is included within the Supplemental Material [21].

Our YIG/Py bilayers are fabricated by magnetron-sputtering Py thin films on 3- $\mu\text{m}$ -thick, single-sided, commercial YIG films grown on double-side-polished  $\text{Gd}_3\text{Ga}_5\text{O}_{12}$  (GGG) substrates using liquid phase epitaxy (LPE). Following earlier recipes to ensure a good YIG/Py interfacial exchange coupling [17], we use *in situ* argon gas rf-bias cleaning for 3 min in the vacuum chamber, to clean the YIG surface before depositing a 30-nm Py layer. In the earlier report [17], we also fabricated and measured

the YIG/SiO<sub>2</sub>/Py and YIG/Cu/Py reference samples. The SiO<sub>2</sub> and the Cu layers can both effectively break the interfacial exchange coupling, thus resulting in a null observation of the magnon-magnon coupled characteristics.

The samples are flipped on a coplanar waveguide (CPW) for broadband microwave excitation. The experimental details of spin-dynamic excitation and magneto-optic detection can be found in our earlier report [17]. We use a heterodyne technique in which a 1550-nm laser light is linearly polarized and modulated at the FMR frequencies simultaneously with the sample's excitation [22–25], and detect the dynamic Faraday and Kerr signals upon the excitation of Py-FMR and YIG's perpendicular standing spin waves (PSSWs). Due to the dispersion relation of YIG and Py, the Py-FMR mode couples to the YIG-PSSW modes and effectively serves as a “lossy cavity.”

Due to the limited spatial overlap, the YIG-PSSW modes couple weakly to the CPW's microwave drive. However, as shown by a typical trace in Fig. 1(c) measured at 4 GHz, through the interfacial exchange coupling, the Py-FMR mode can efficiently excite the PSSW modes under its envelope (50–250 Oe), and resonantly enhancing the YIG dynamics. At the same time, the YIG PSSW modes strongly modulate the Py resonance profile, exhibiting the “MIT dip”, which is a sharp reduction to the Py resonance. The magneto-optic signal,  $V$ , with the phase information, are obtained by the lock-in's in-phase  $X$  ( $\text{Re}[V]$ ) and quadrature  $Y$  ( $\text{Im}[V]$ ), which are further used to calculate the total amplitude,  $\text{Amp}[|V|] = \sqrt{X^2 + Y^2}$ . By considering a series of YIG harmonic oscillators coupled with the Py oscillator, the coupled spin dynamics in the MIT regime can be phenomenologically modeled, and the measured complex magneto-optic signal,  $V$ , can be expressed as

$$V = \frac{A e^{i(\phi_L - \phi_m)}}{i(H_{\text{FMR}}^{\text{Py}} - H) - \Delta H_{\text{Py}} + \Sigma_n [g^2 / i(H_{\text{PSSW},n}^{\text{YIG}} - H) - \Delta H_{\text{YIG},n}]}, \quad (1)$$

where  $A$  is the total signal amplitude,  $H_{\text{FMR}}^{\text{Py}}$  and  $H_{\text{PSSW}}^{\text{YIG}}$  is the resonance field of Py and YIG-PSSWs, respectively,  $\Delta H_{\text{YIG}(Py)}$  is the half-width-half-maximum linewidth,  $n$  is the PSSW mode-index number, and  $g$  is the fieldlike coupling strength from the interfacial exchange. According to our previous reports [16,17], the YIG and Py are antiferromagnetically coupled at the interface.  $\phi_L$  is the phase accumulated due to the optical path length, and  $\phi_m$  is the magnetization phase. More details regarding the physical contributions to  $\phi_L$  and  $\phi_m$  can be found in the earlier reports [17,24]. To examine the magnetic field tunability of the magnon-magnon coupled spectra, we perform

measurements on the YIG/Py(30-nm) sample under three experimental configurations: OOP rotating field, IP rotating field, and IP rotating field with a static OOP disturbing field by using a permanent magnet. All experiments are performed at room temperature.

## III. RESULTS AND DISCUSSIONS

### A. Out-of-plane magnetic field dependence

Earlier experimental reports have shown an enhanced magnon-magnon coupling due to the introduction of out-of-plane magnetic field, magnetic anisotropy, and

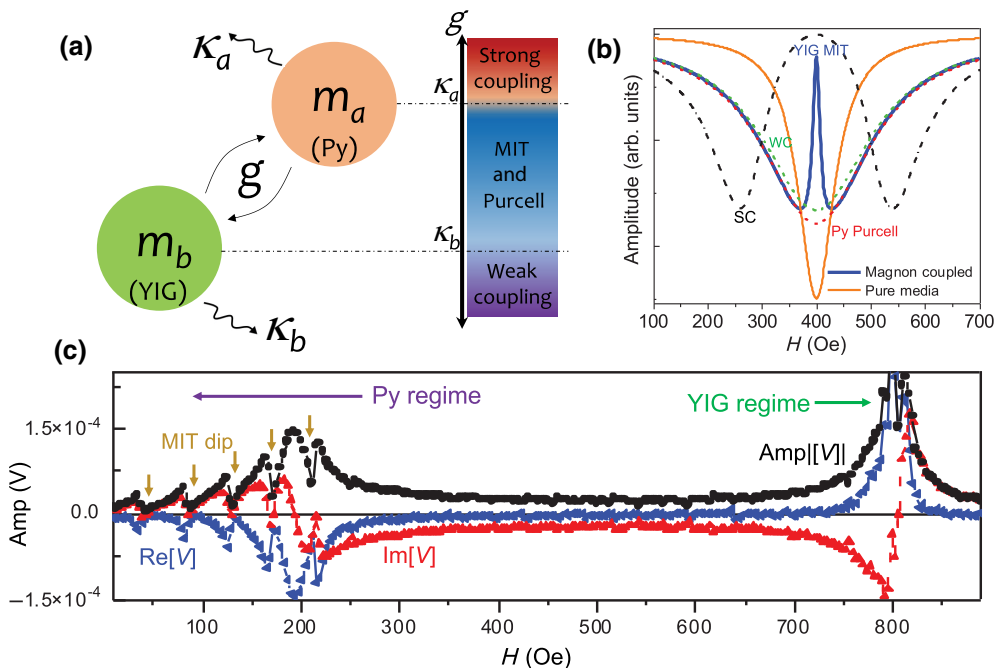


FIG. 1. (a) Schematics of the linearly coupled magnon-magnon system:  $m_a(\text{Py}) \rightleftharpoons m_b(\text{YIG})$ .  $g$ ,  $\kappa_a$ ,  $\kappa_b$  are the coupling strength and dissipation rates of the respective magnon subsystems. Different coupling regimes are characterized and separated by the relative strength between the coupling rate and dissipation rates of the two magnon subsystems. (b) Illustration of the coupled-mode spectra in the MIT-Purcell regime ( $\kappa_b < g < \kappa_a$ ). In the field domain, the mode hybridization leads to an abrupt suppression of the absorption at a certain field window. Such a transparency window, whose bandwidth is determined by the low-loss mode (YIG), can be observed in the broad resonance of the other lossy mode (Py). Reciprocally, the lossy mode exhibits enhanced decay due to the Purcell effect. Such resonant phenomena can be controlled by an external magnetic field. As a comparison, the modeled trace for the case of strong coupling (SC) and weak coupling (WC) are also plotted. (c) An example magneto-optical signal trace of YIG/Py(30 nm) showing the lineshapes of the in-phase  $X$  ( $\text{Re}[V]$ ) and quadrature  $Y$  ( $\text{Im}[V]$ ), and the total amplitude,  $\text{Amp}[|V|] = \sqrt{X^2 + Y^2}$ , measured at 4 GHz at  $\theta = 0^\circ$ ,  $\phi = 0^\circ$  ( $h \perp H$ ). The low-field (0–300 Oe) regime corresponds to the Py-FMR regime, where the hybridized YIG PSSW modes strongly modulate the Py resonance profile, exhibiting the “MIT dip” (vertical arrows). The high-field (700–900 Oe) regime corresponds to the YIG-FMR regime.

Dzyaloshinskii-Moriya interaction (DMI) in magnetic multilayers, particularly in the synthetic antiferromagnet (SAF) systems [26–29]. It is theoretically explained by the additional symmetry breaking due to the out-of-plane effective field that increases the magnon-magnon interaction [30]. Beyond the SAFs where the magnetic layers are coupled by the Ruderman-Kittel-Kasuya-Yosida (RKKY) interaction, it is also worthwhile to investigate similar effects in the direct exchange-coupled YIG/Py, which has been a prototypical magnon-magnon system. In addition, since the YIG and Py has distinct magnetic characteristics, it is useful to examine how the magnetization geometry of the two layers influences their magnon-magnon coupled spin dynamics.

Our measurement setup and dataset for the OOP field experiment are shown in Fig. 2. The external magnetic field generated by the electromagnet can be rotated out of plane ( $x$ - $y$ ), at an angle  $\phi$  with respect to the sample plane ( $y$ - $z$ ), as illustrated in Fig. 2(a). The Oersted field,  $h$ , supplied by the CPW, is along  $z$ . We scan the frequency,  $f$ ,

and magnetic field,  $H$ , around the Py-FMR (MIT regime), and plot the  $\text{Re}[V(f, H)]$  map at incremental  $\phi$  angles from  $0^\circ$  to  $60^\circ$ , at a step of  $15^\circ$ . Figure 2(b) shows the contour plots of the MIT spectra at  $0^\circ$ ,  $30^\circ$ , and  $60^\circ$ . The two-dimensional plots are generated from the individual  $\text{Re}[V]$  spectra acquired by sweeping the magnetic field at a given frequency (from 4 to 4.15 GHz). From the contour plots, it can be seen that the Py-FMR is strongly modulated by a series of sharp YIG PSSW modes, showing a series of MIT dip. A group of 5–6 PSSWs can be clearly identified under the Py uniform excitation. Due to the much lower resonance field of Py compared to YIG, see Fig. 1(c), these PSSWs are usually higher-index modes, typically with an index number,  $n \sim 30$ –40, with the corresponding wave numbers  $k = n\pi/d_{\text{YIG}} \sim 31.5$ – $42.0 \mu\text{m}^{-1}$ , where  $d_{\text{YIG}}$  is the YIG thickness, according to our previous report [17].

To analyze the coupling strength  $g$ , we choose the two to three PSSW modes that are close to the center of the Py resonance envelope, and fit the experimental  $V(H)$  traces with Eq. (1). The coupling  $g$ , and the dissipation rates for YIG

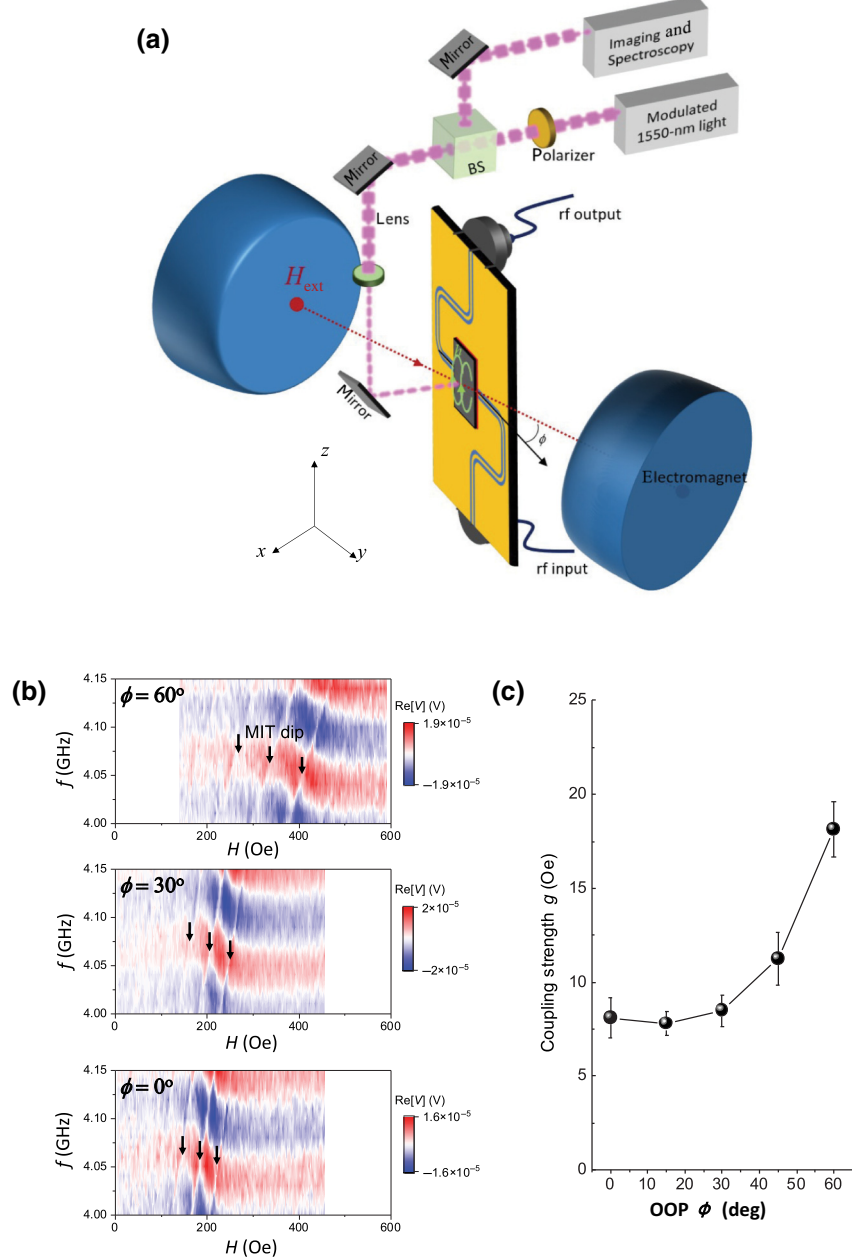


FIG. 2. (a) Schematics of the experimental magneto-optic setup for OOP magnetic field configuration. A 1550-nm light is sourced and modulated by fiber-optic components before entering the real space. Key components in the real space includes a polarizer, a beam splitter (BS), a focus lens, and mirrors for detouring the light path. The microwave excitation for the sample is achieved by a coplanar waveguide in a flip-chip configuration. Light passes through the YIG layer and is retroreflected against the opaque Py layer, before it is directed towards a balancing photodiode and subsequent signal analysis. (b) Example contour plots of the measured  $\text{Re}[V(f, H)]$  at  $\phi = 0^\circ$ ,  $30^\circ$ , and  $60^\circ$ , where the MIT dips are marked by the arrows. (c) OOP  $\phi$  angular dependence of the extracted coupling strength  $g$ .

and Py are subsequently extracted. In the field domain, the lower limit of the field linewidth for the lossy magnon cavity of Py is approximately 30.0 Oe, and the upper limit of the YIG linewidth is approximately 2.0 Oe. On the other hand, the extracted coupling  $g$ , as plotted in Fig. 2(c), is in the range of approximately 7.0–20.0 Oe. Therefore, the

hybrid system is confirmed in the MIT coupling regime, satisfying  $\kappa_{\text{YIG}} < g < \kappa_{\text{Py}}$ . Notably, the coupling strength  $g$  increases with increasing OOP angle,  $\phi$ . At  $\phi = 60^\circ$ , the coupling is more than double that of the IP case ( $\phi = 0^\circ$ ). Such an angular dependence is in a general agreement with the magnon coupled acoustic and optic modes in the SAFs

reported earlier, which also features an antiferromagnetic coupling at the interface, but via the RKKY interaction [26–29].

In order to verify the tunable coupling between the PSSW modes of YIG and the FMR mode of Py, micromagnetic simulations are performed to numerically solve the Landau-Lifshitz-Gilbert equation by using MuMax3 [31], with the effective magnetic field including contributions from the interlayer exchange field, the intralayer exchange field, the demagnetization field, and the external field. The strength of the interlayer exchange interaction between the YIG and the Py layers is determined by the exchange energy density  $J$ . The modeled thickness of the Py and YIG layers are the same as in the experiment:  $t_{\text{Py}} = 30 \text{ nm}$  and  $t_{\text{YIG}} = 3000 \text{ nm}$ , respectively. The whole Py/YIG bilayer structure with size  $200 \times 200 \times 3030 \text{ nm}^3$  is discretized into  $10 \times 10 \times 1212$  cells. The periodic boundary conditions are applied in the in-plane two directions along the  $y$ - $z$ . The material parameters used in simulations are as follows: for Py layer,  $M_s^{\text{Py}} = 8.6 \times 10^5 \text{ A/m}$ ,  $A_{\text{ex}}^{\text{Py}} = 1.3 \times 10^{-11} \text{ J/m}$ , and  $\alpha_{\text{Py}} = 0.01$ ; for YIG layer,  $M_s^{\text{YIG}} = 1.4 \times 10^5 \text{ A/m}$ ,  $A_{\text{ex}}^{\text{YIG}} = 3.5 \times 10^{-12} \text{ J/m}$ , and  $\alpha_{\text{YIG}} = 5 \times 10^{-4}$ . The strength of interlayer exchange interaction is determined by  $J = 0.3 \times 10^{-3} \text{ J/m}^2$ .

To excite PSSW modes in the YIG layer, a driving field  $h_z(t)$  is locally applied in the bottom-most layer of the Py along the  $z$  axis [32]. The  $h_z(t)$  is in the form of “sinc” function [33]:  $h_z(t) = h_0 \sin[2\pi f(t - t_0)]/2\pi f(t - t_0)$ , with the cutoff frequency  $f = 50 \text{ GHz}$ , the offset time  $t_0 = 0.25 \text{ ns}$ , and the amplitude  $h_0 = 1 \text{ mT}$ . The spatially averaged magnetization of all cells is recorded every 10 ps during the total simulation time of 100 ns. The spin-wave spectra can be obtained by Fourier transforming the out-of-plane component of the magnetization in the Py layer.

Figure 3(a) illustrates the oblique magnetic field effect to the magnetization distribution of the YIG/Py bilayer. The simulated microwave absorption spectra and the  $f$ - $H$  dispersion curves are shown in Figs. 3(b) and 3(c), respectively, for representative OOP angles,  $\phi = 0^\circ$ ,  $30^\circ$ , and  $45^\circ$ . It is found that the splitting of the hybridized modes between the uniform mode of Py and the PSSW modes of YIG is enhanced by increasing the  $\phi$  angle. To better understand the splitting, the coupling strength  $g$  is extracted from the microwave absorption spectra according to Eq. (1). The simulated  $g$  value is 7.51, 8.75, and 11.31 Oe, at  $\phi = 0^\circ$ ,  $30^\circ$ , and  $45^\circ$ , respectively. Figure 3(d) shows that the  $g$  increases with increasing  $\phi$  from  $0^\circ$  to  $60^\circ$ , which is consistent with the experimental observation shown in Fig. 2.

Such a dependence can be understood by the geometrical factor of YIG and Py macrospins as well as the external field-induced noncollinear magnetization distributions along the thickness direction of the YIG/Py bilayer as shown in Fig. 3(a). When the external field  $H$  is applied

out of plane, the magnetization in Py is estimated always in the plane in the studied field range. However, the magnetization of YIG along the thickness direction is spatially dependent on the distance to Py and gradually tilting towards  $H$ . The further away from the Py, the magnetization in the YIG is closer to the direction of  $H$ . The larger the difference between the magnetization of Py and YIG, the larger the coupling strength  $g$ , which results from the  $H$ -induced spatial symmetry breaking. Similar observations have been also reported in the magnetic bilayer of Co wires deposited on YIG film [18].

From a theory perspective, a comprehensive analytical model would be difficult to develop due to the many factors that may change with increasing the OOP  $\phi$  angle, such as the mode ellipticities, excitation of PSSWs with different mode index  $n$ , and the dipolar interactions [18,29,34–36]. On the other hand, our earlier work [17] and the subsequent sections (with in-plane angle dependence) suggest that the coupling strength  $g$  is a weak function of the PSSW mode number  $n$  at higher indices,  $n > 25$ . In addition, the contribution to the coupling by the change of the precessional ellipticity is estimated to be less than approximately 3%. However, one factor that has not been well discussed so far is the additional dipolar interaction that may be caused by the obliquely applied magnetic field. To this end, we have theoretically modeled the effect of such a dipolar interaction to the coupling between the Py and YIG spin-wave mode, which can be found within the Supplemental Material [21].

By solving the matrix element of the dipolar interaction calculated for complex spin-wave profiles of the interacting modes, we find an additional, dipolar coupling strength,  $g_{\text{dip}}$ , that depends on the magnetization directions, due to the geometrical restriction of the excited spin-wave modes. A theoretical relationship between the coupling and the internal OOP magnetization angles of Py ( $\phi_{\text{Py}}$ ) and YIG ( $\phi_{\text{YIG}}$ ) can be derived as

$$g_{\text{dip}} = g_0 + \kappa_0 h(\phi_{\text{YIG}}, \phi_{\text{Py}}), \quad (2)$$

where  $g_0$  and  $\kappa_0$  are geometrical-independent constants (details are included within the Supplemental Material [21]). The geometrical function,  $h(\phi_{\text{YIG}}, \phi_{\text{Py}})$ , can be expressed as  $h(\phi_{\text{YIG}}, \phi_{\text{Py}}) = 1 - \cos(\phi_{\text{YIG}}) \cos(\phi_{\text{Py}}) + \frac{1}{2} \sin(\phi_{\text{YIG}}) \sin(\phi_{\text{Py}})$ , and this angular function  $h(\phi_{\text{YIG}}, \phi_{\text{Py}})$  is an increasing function of  $\phi_{\text{YIG}}$ . On the other hand, due to a much higher magnetization in the Py layer, the OOP magnetization angle of Py,  $\phi_{\text{Py}}$ , will be smaller than  $\phi_{\text{YIG}}$ . Therefore, the OOP oblique field to the YIG/Py bilayer should result in a net enhancement of the dipolar coupling between the YIG’s spin-wave modes and the Py-FMR. A detailed theoretical description can be found within the Supplemental Material [21].

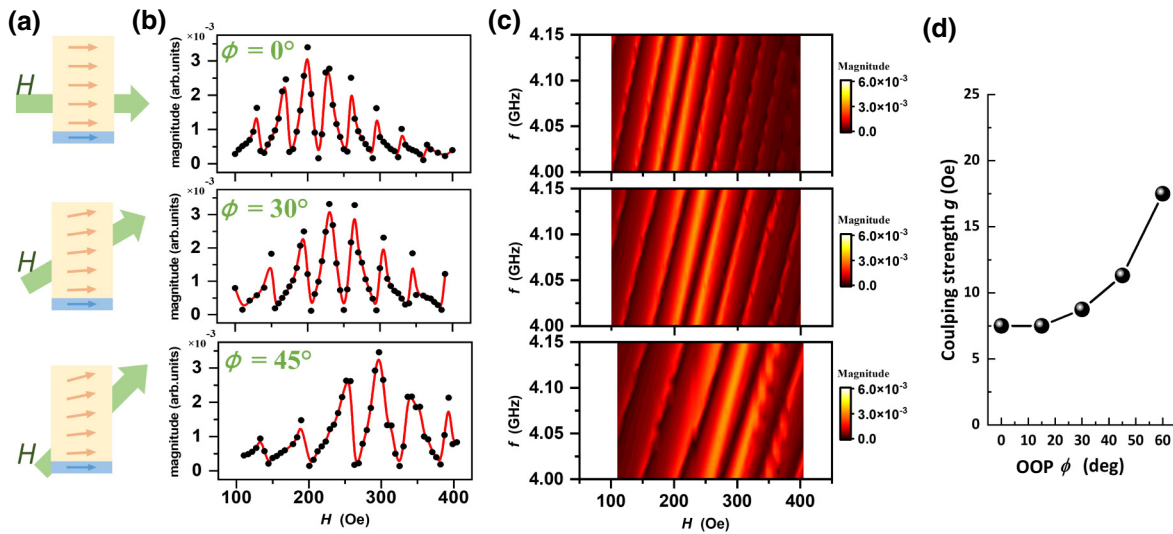


FIG. 3. (a) Illustration of the oblique magnetic field effect: the blue and yellow areas represent the Py/YIG layer with arrows indicating the direction of magnetization. Green arrows indicate the direction of the external magnetic field  $H$ . (b) Simulated microwave absorption spectrum at 4.1 GHz for representative OOP  $\phi$  angles:  $\phi = 0^\circ$ ,  $30^\circ$ , and  $45^\circ$ , reproducing the experimentally observed MIT dips. (c) Corresponding color contour plots of the simulated  $f$ - $H$  dispersion from 4.0–4.15 GHz:  $\phi = 0^\circ$ ,  $30^\circ$ , and  $45^\circ$ . (d) Simulated dependence of the coupling strength  $g$  on the OOP  $\phi$  angle.

## B. In-plane magnetic field dependence

Next, we discuss the measurement setup and dataset for the IP field experiment. Generally, for the PSSWs that are of interest here, one would not expect any in-plane field dependence due to the fact that the wave number is pointing out of plane, and both the YIG and Py are sufficiently soft. However, due to our CPW excitation, the rf field is fixed along  $x$  (in the IP configuration), it would be useful then to examine and verify any possible dependence that may be caused by the relative orientation between the rf field and the magnetization.

Our measurement setup and dataset for the IP field experiment are summarized in Fig. 4. In this configuration, the sweeping magnetic field supplied by the electromagnet can be rotated in plane ( $x$ - $y$ ), at an angle  $\theta$ , with respect to the central CPW signal line (along  $y$ ), see Fig. 4(a). The Oersted field,  $h$ , supplied by the CPW, is along  $x$ . Similarly, we scan the frequency and magnetic field around the MIT regime, and at incremental  $\theta$  angles from  $0^\circ$  to  $90^\circ$ , at a step of  $15^\circ$ . In such an IP configuration, we can also optionally introduce an additional OOP disturbing field,  $H_p$ , from the back of the sample, via an axially magnetized permanent magnet placed on a micropositioner, to further modify the MIT spectra (results to be discussed later).

Figure 4(b) shows example  $V(H)$  traces at 4 GHz measured at  $\theta = 15^\circ$ ,  $45^\circ$ , and  $75^\circ$  around the Py-FMR regime. We again analyze the coupling strength  $g$  via fitting the hybridized PSSW modes near the center of the Py-FMR in the  $V(H)$  curves with Eq. (1). The extracted coupling,  $g$ , as plotted in Fig. 4(c), is approximately 7.0–10.0

Oe, and has indicated a negligible IP  $\theta$  angular dependence, despite a global signal amplitude attenuation as  $\theta$  increases. Since the interfacial exchange (the dominant driving force) has a negligible anisotropy and both YIG and Py are soft magnets, the anisotropic excitation caused by the CPW signal line plays a negligible role in the magnon-magnon hybridization. In addition, with both the YIG and Py macrospins aligned in plane, the influence from the geometrical factor and the possibly associated dipolar interaction do not contribute to additional coupling terms.

We note that earlier reports in dealing with SAFs have suggested a nontrivial IP angular dependence along with a wave-number dependence of the coupling strength  $g$  [26–28]. Here, although using different  $g$  values for the  $V(H)$  fitting can in principle lead to an improved fitting result, we do not find a convincing  $k$ -dependent coupling  $g$ , which is also expected for the hybridized PSSW modes. This is because the wave number of the PSSWs is primarily pointing out of plane, and the dipolar coupling between the PSSWs and the in-plane Py are sufficiently weak [32]. Besides, due to the large difference in the magnetization of YIG and Py, the PSSW modes that are actively coupled to the Py uniform mode are of higher index ( $n \sim 30$ –40), and their dipolar field is much less than the uniform mode and even those long-wavelength (smaller  $n$ ) PSSW modes [17]. However, this does not exclude the possible contribution of dipolar-enhanced coupling when the magnetization is tilted out of plane, as we discuss in the OOP case earlier.

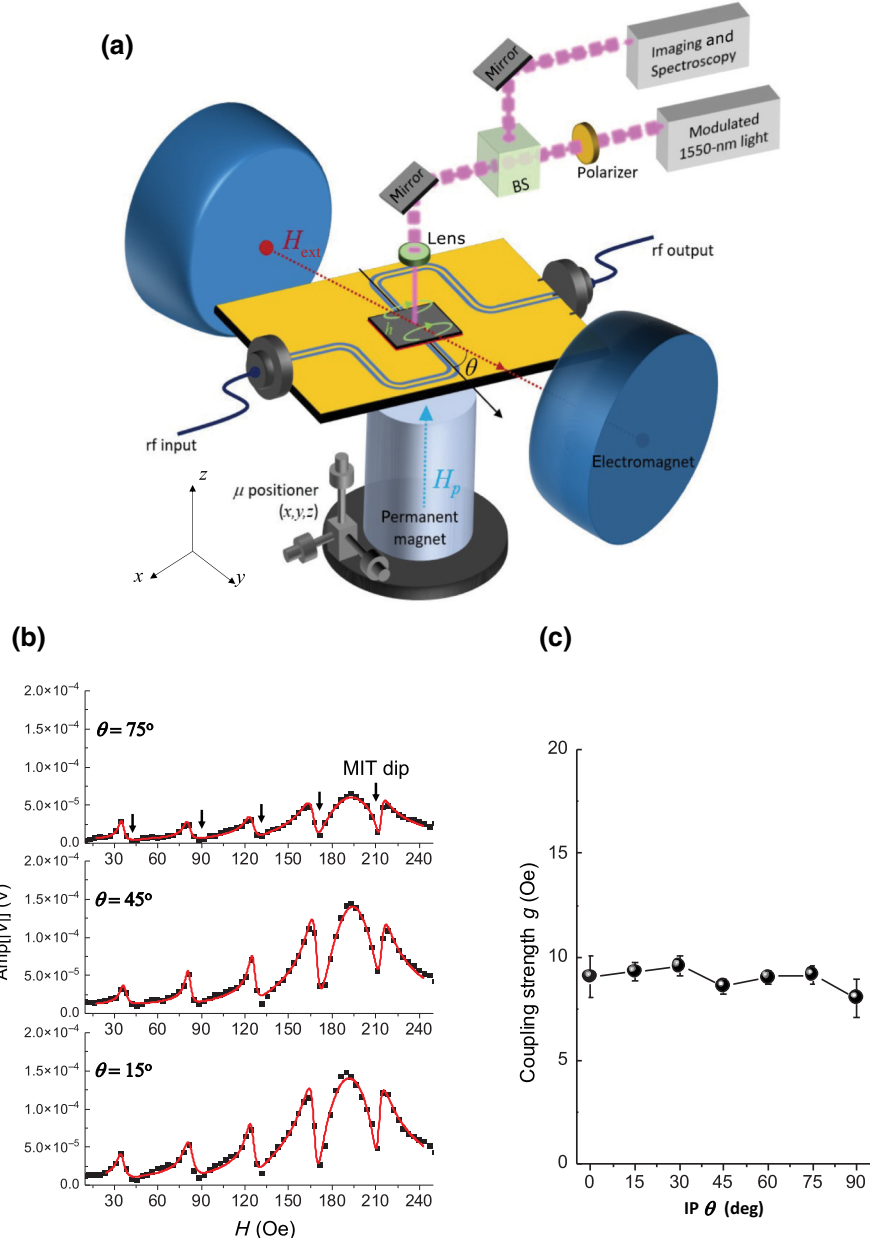


FIG. 4. (a) Schematics of the experimental magneto-optic setup for IP magnetic field configuration (with optional OOP disturbing fields). (b) Example signal traces of  $V(H)$  measured at 4 GHz (dots) and the corresponding fitting curves (lines) following the Eq. (1), at  $\theta = 15^\circ, 45^\circ$ , and  $75^\circ$ . A total of five MIT dips can be observed (arrows). As the  $\theta$  increases, the amplitude of the Py-FMR and the MIT dip decrease at approximately the same rate, therefore leading to a negligible dependence of  $g$  versus  $\theta$ . (c) The extracted IP  $\theta$  angular dependence of the extracted coupling strength  $g$ .

### C. Out-of-plane bias magnetic field

We then discuss the effect of introducing an OOP disturbing field,  $H_p$  on the MIT spectra and the coupling  $g$  in the IP measurement configuration. Different from the OOP field sweeping discussed earlier in Sec. III A, our experiment here examines how a static OOP bias field, mimicking effectively an unidirectional anisotropy, may influence the magnon-magnon coupled characteristics. In

real-world material systems, such an effective field may be provided by either a magnetic anisotropy or a DMI field.

The disturbing field is provided by a large diameter (0.5 in. diameter), axially magnetized, permanent magnet that is fixed on a micropositioner, see Fig. 4(a), and placed in close proximity with the sample and CPW stack from the backside. Such a static field serves as a constant “bias field” to the same field-sweep experiment described

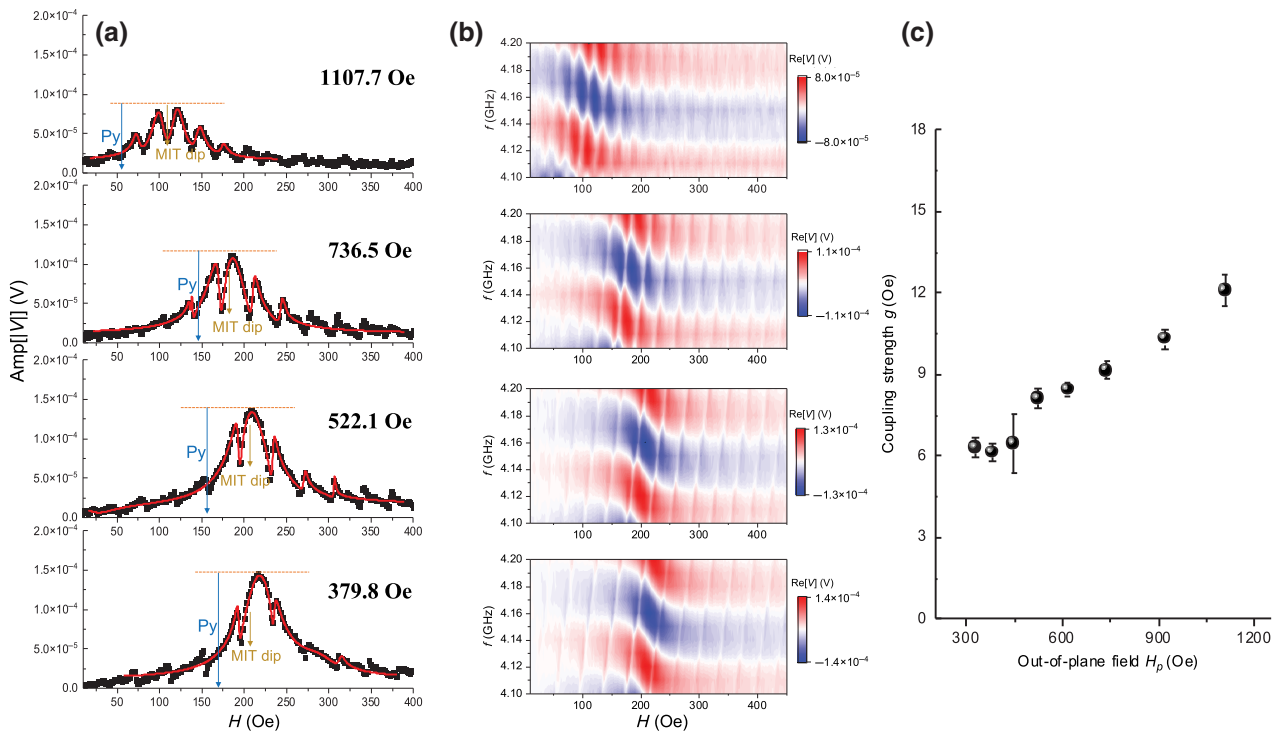


FIG. 5. (a) Example  $V(H)$  signal traces measured at 4.16 GHz (dots) and the corresponding fitting curves (lines) following the Eq. (1), and (b) corresponding  $\text{Re}[V(f, H)]$  contour plots, at selective  $H_p$  values: 379.8, 522.1, 736.5, and 1107.7 Oe. In (a), the modulation effect to the Py-FMR profile can be visualized by directly comparing the total Py amplitude and the modulation depth (the MIT dip) caused by the hybrid YIG-PSSW modes (arrows). (c) The  $H_p$  dependence of the extracted coupling strength  $g$ .

in Fig. 4. By adjusting the position of the magnet (primarily along  $z$ ), the magnitude of  $H_p$  can be tuned. After first performing a calibration of the magnetic field, we find a uniform-field range of approximately 350–1200 Oe, which corresponds to a sample-magnet gap distance in the range of approximately 0.5–7.0 mm. We perform similar measurements in the IP configuration under such a static disturbing field at a fixed  $\theta = 0^\circ$ , and the results are summarized in Fig. 5.

Figure 5(a) shows example  $V(H)$  traces measured at 4.16-GHz at selective  $H_p$  values, 379.8, 522.1, 736.5, and 1107.7 Oe. Increasing the magnitude of  $H_p$  leads to an overall shift of the MIT regime towards lower field range, due to the modification to the Py-FMR dispersion. In addition, the magnon-magnon coupling becomes stronger as  $H_p$  increases, which is evidenced by the enhanced modulation effect to the Py-FMR profile caused by the hybrid PSSW modes. Such a modulation effect can be visualized simply by comparing the total Py amplitude and the modulation depth (the MIT dip) caused by the hybridization. Figure 5(b) shows the corresponding contour plots of  $\text{Re}[V(f, H)]$  at the same  $H_p$  values as in Fig. 5(a). The frequency range is scanned around the MIT regime, from 4.1 to 4.2 GHz, and the field is swept from 0 to 450 Oe.

Similar to the above OOP and IP cases, we can also analyze the MIT spectra under such a bias OOP field  $H_p$ ,

and extract a coupling strength  $g$  via fitting the hybridized PSSW modes near the center of the Py-FMR in the  $V(H)$  curves with Eq. (1). The extracted coupling,  $g$  is further plotted in Fig. 5(c). For  $H_p$  values below approximately 500.0 Oe, no significant effect can be found. However, for  $H_p$  values above approximately 500.0 Oe, a robust enhancement of the coupling  $g$  is observed, which steadily increases as  $H_p$  increases. This result echos our earlier experiment with the OOP configuration. The enhanced coupling  $g$  could be again likewise attributed to the similar symmetry breaking and the geometrical consideration of YIG and Py macrospins, as well as the enhanced dipolar interactions due to the tilted magnetization. Finally, we note that our experiment with the OOP disturbing field also reflects a tunable signal response and a great spectrum sensitivity at the MIT regime, which may be found useful in magnetic sensing applications with magnon-magnon coupled systems.

#### IV. CONCLUSION

In summary, we experimentally study the magnetic field tunability of the magnetically induced transparency spectra in YIG/Py magnon-magnon coupled bilayers. By probing the magneto-optic effects of Py and YIG, we identify clear features of MIT spectra induced by the mode

hybridization between the FMR of Py and the PSSWs of YIG. By changing the external magnetic field orientation out of plane, we observe a tunable coupling strength between the YIG's spin-wave modes and the Py's uniform mode. Such a tunable coupling can be understood by a geometrical consideration of the oblique magnetization vectors of the Py and YIG, which enhances the coupling via an additional coupling effect from the dipolar interaction. On the other hand, rotating the magnetic field in plane results in no observable changes to the magnon-magnon coupling strength, which agrees with the standing-wave nature of the excited spin-wave modes. Further, by introducing a static bias magnetic field using a permanent magnet, we reconfirm such a geometrical effect to the coupling strength under an out-of-plane magnetic field component. Our reported experiments may be found useful for future studies on the tunable coherent phenomena with hybrid magnonic platforms.

## ACKNOWLEDGMENTS

The experimental measurement and theoretical modeling at Oakland University is supported by the U.S. National Science Foundation under Grant No. ECCS-1941426. The sample fabrication and preparation at Argonne National Laboratory is supported by U.S. DOE, Office of Science, Materials Sciences and Engineering Division. The micromagnetic simulations at Nanjing Normal University is supported by the National Natural Science Foundation of China (Grant No. 12074189). Z.-L.X. acknowledges funding support from the U.S. National Science Foundation under Grant No. DMR-1901843. We thank Dr. Vivek Amin and Zhizhi Zhang for fruitful discussions and Mr. Lei Zhang and Dr. Cassie Ward for structural and surface characterizations. Part of the characterization also made use of the PXDR facility that is partially funded by NSF under Grant No. MRI-1427926 at Wayne State University.

- 
- [1] D. Lachance-Quirion, Y. Tabuchi, A. Gloppe, K. Usami, and Y. Nakamura, Hybrid quantum systems based on magnonics, *Appl. Phys. Express* **12**, 070101 (2019).
  - [2] M. Harder and C.-M. Hu, Cavity spintronics: An early review of recent progress in the study of magnon-photon level repulsion, *Solid State Phys.* **70**, 47 (2018). R. Stamps and R. Camley (Ed.), Academic Press.
  - [3] B. Bhoi and S.-K. Kim, Photon-magnon coupling: Historical perspective, status, and future directions, *Solid State Phys.* **69**, 1 (2019). R. Stamps and H. Schultheiss (Ed.), Academic Press.
  - [4] D. D. Awschalom, *et al.*, Quantum engineering with hybrid magnonics systems and materials, *IEEE Trans. Quantum Eng.* **2**, 5500836 (2021).
  - [5] Y. Li, W. Zhang, V. Tyberkevych, W.-K. Kwok, A. Hoffmann, and V. Novosad, Hybrid magnonics: Physics, circuits, and applications for coherent information processing, *J. Appl. Phys.* **128**, 130902 (2020).
  - [6] Y. Tabuchi, S. Ishino, A. Noguchi, T. Ishikawa, R. Yamazaki, K. Usami, and Y. Nakamura, Coherent coupling between a ferromagnetic magnon and a superconducting qubit, *Science* **349**, 405 (2015).
  - [7] L. McKenzie-Sell, J. Xie, C.-M. Lee, J. W. A. Robinson, C. Ciccarelli, and J. A. Haigh, Low-impedance superconducting microwave resonators for strong coupling to small magnetic mode volumes, *Phys. Rev. B* **99**, 140414 (2019).
  - [8] Y. Li, T. Polakovic, Y.-L. Wang, J. Xu, S. Lendinez, Z. Zhang, J. Ding, T. Khaire, H. Saglam, R. Divan, J. Pearson, W. K. Kwok, Z. Xiao, V. Novosad, A. Hoffmann, and W. Zhang, Strong Coupling between Magnons and Microwave Photons in On-Chip Ferromagnet-Superconductor Thin-Film Devices, *Phys. Rev. Lett.* **123**, 107701 (2019).
  - [9] J. T. Hou and L. Liu, Strong Coupling Between Microwave Photons and Nanomagnet Magnons, *Phys. Rev. Lett.* **123**, 107702 (2019).
  - [10] H. Huebl, C. W. Zollitsch, J. Lotze, F. Hocke, M. Greifenstein, A. Marx, R. Gross, and S. T. B. Goennenwein, High Cooperativity in Coupled Microwave Resonator Ferromagnetic Insulator Hybrids, *Phys. Rev. Lett.* **111**, 127003 (2013).
  - [11] L. Bai, M. Harder, Y. P. Chen, X. Fan, J. Q. Xiao, and C. M. Hu, Spin Pumping in Electrodynamically Coupled Magnon-Photon Systems, *Phys. Rev. Lett.* **114**, 227201 (2015).
  - [12] X. Zhang, C.-L. Zou, L. Jiang, and H. X. Tang, Strongly Coupled Magnons and Cavity Microwave Photons, *Phys. Rev. Lett.* **113**, 156401 (2014).
  - [13] X. Zhang, C.-L. Zou, N. Zhu, F. Marquardt, L. Jiang, and H. X. Tang, Magnon dark modes and gradient memory, *Nat. Commun.* **6**, 8914 (2015).
  - [14] S. Klingler, V. Amin, S. Geprägs, K. Ganzhorn, H. Maier-Flaig, M. Althammer, H. Huebl, R. Gross, R. D. McMichael, M. D. Stiles, S. T. B. Goennenwein, and M. Weiler, Spin-Torque Excitation of Perpendicular Standing Spin Waves in Coupled YIG/Co Heterostructures, *Phys. Rev. Lett.* **120**, 127201 (2018).
  - [15] H. Qin, S. J. Hamalainen, and S. van Dijken, Exchange-torque-induced excitation of perpendicular standing spin waves in nanometer-thick YIG films, *Sci. Rep.* **8**, 5755 (2018).
  - [16] Y. Li, W. Cao, V. P. Amin, Z. Zhang, J. Gibbons, J. Sklenar, J. Pearson, P. M. Haney, M. D. Stiles, W. E. Bailey, V. Novosad, A. Hoffmann, and W. Zhang, Coherent Spin Pumping in a Strongly Coupled Magnon-Magnon Hybrid System, *Phys. Rev. Lett.* **124**, 117202 (2020).
  - [17] Y. Xiong, Y. Li, M. Hammami, R. Bidhanapally, J. Sklenar, X. Zhang, H. Qu, G. Srinivasan, J. Pearson, A. Hoffmann, V. Novosad, and W. Zhang, Probing magnon-magnon coupling in exchange coupled  $\text{Y}_3\text{Fe}_5\text{O}_{12}$ /Permalloy bilayers with magneto-optical effects, *NPG Sci. Rep.* **10**, 12548 (2020).
  - [18] J. Chen, C. Liu, T. Liu, Y. Xiao, K. Xia, G. E. W. Bauer, M. Wu, and H. Yu, Strong Interlayer Magnon-Magnon Coupling in Magnetic Metal-Insulator Hybrid Nanostructures, *Phys. Rev. Lett.* **120**, 217202 (2018).

- [19] V. D. Poimanov, A. N. Kuchko, and V. V. Kruglyak, Emission of coherent spin waves from a magnetic layer excited by a uniform microwave magnetic field, *J. Phys. D: Appl. Phys.* **52**, 135001 (2019).
- [20] V. D. Poimanov, A. N. Kuchko, and V. V. Kruglyak, Magnetic interfaces as sources of coherent spin waves, *Phys. Rev. B* **98**, 104418 (2018).
- [21] See Supplemental Material at <http://link.aps.org/supplemental/10.1103/PhysRevApplied.17.044010> for additional details on the experimental setup, theoretical analysis, and supporting sample characterizations.
- [22] Y. Li, H. Saglam, Z. Zhang, R. Bidhanapally, Y. Xiong, J. E. Pearson, V. Novosad, H. Qu, G. Srinivasan, A. Hoffmann, and W. Zhang, Simultaneous Optical and Electrical Spin-Torque Magnetometry with Phase-Sensitive Detection of Spin Precession, *Phys. Rev. Appl.* **11**, 034047 (2019).
- [23] Y. Li, F. Zeng, H. Saglam, J. Sklenar, J. E. Pearson, T. Sebastian, Y. Wu, A. Hoffmann, and W. Zhang, Optical detection of phase-resolved ferromagnetic resonance in epitaxial FeCo thin films, *IEEE Trans. Magn.* **55**, 6100605 (2019).
- [24] Y. Xiong, Y. Li, R. Bidhanapally, J. Sklenar, M. Hammami, S. Hall, X. Zhang, P. Li, J. E. Pearson, T. Sebastian, G. Srinivasan, A. Hoffmann, H. Qu, V. Novosad, and W. Zhang, Detecting phase-resolved magnetization dynamics by magneto-optic effects at 1550 nm wavelength, *IEEE Trans. Magn.* **57**, 4300807 (2021).
- [25] Y. Shiota, R. Hisatomi, T. Moriyama, A. S. Samardak, and T. Ono, Inhomogeneous magnetic properties characterized by simultaneous electrical and optical detection of spin-torque ferromagnetic resonance, *Appl. Phys. Lett.* **119**, 192409 (2021).
- [26] D. MacNeill, J. T. Hou, D. R. Klein, P. Zhang, P. Jarillo-Herrero, and L. Liu, Gigahertz Frequency Antiferromagnetic Resonance and Strong Magnon-Magnon Coupling in the Layered Crystal CrCl<sub>3</sub>, *Phys. Rev. Lett.* **123**, 047204 (2019).
- [27] Y. Shiota, T. Taniguchi, M. Ishibashi, T. Moriyama, and T. Ono, Tunable Magnon-Magnon Coupling Mediated by Dynamic Dipolar Interaction in Synthetic Antiferromagnets, *Phys. Rev. Lett.* **125**, 017203 (2020).
- [28] A. Sud, C. W. Zollitsch, A. Kamimaki, T. Dion, S. Khan, S. Iihama, S. Mizukami, and H. Kurebayashi, Tunable magnon-magnon coupling in synthetic antiferromagnets, *Phys. Rev. B* **102**, 100403(R) (2020).
- [29] J. Sklenar and W. Zhang, Self-Hybridization and Tunable Magnon-Magnon Coupling in van der Waals Synthetic Magnets, *Phys. Rev. Appl.* **15**, 044008 (2021).
- [30] M. Li, J. Lu, and W. He, Symmetry breaking induced magnon-magnon coupling in synthetic antiferromagnets, *Phys. Rev. B* **103**, 064429 (2021).
- [31] A. Vansteenkiste, J. Leliaert, M. Dvornik, M. Helsen, F. Garcia-Sanchez, and B. Van Waeyenberge, The design and verification of MuMax3, *AIP Adv.* **4**, 107133 (2014).
- [32] Z. Zhang, H. Yang, Z. Wang, Y. Cao, and P. Yan, Strong coupling of quantized spin waves in ferromagnetic bilayers, *Phys. Rev. B* **103**, 104420 (2021).
- [33] F. S. Ma, H. S. Lim, Z. K. Wang, S. N. Piramanayagam, S. C. Ng, and M. H. Kuok, Micromagnetic study of spin wave propagation in bicomponent magnonic crystal waveguides, *Appl. Phys. Lett.* **98**, 153107 (2011).
- [34] T. Jeffrey, W. Zhang, and J. Sklenar, Effect of dipolar interaction on exceptional points in synthetic layered magnets, *Appl. Phys. Lett.* **118**, 202401 (2021).
- [35] C. Dai and F. Ma, Strong magnon-magnon coupling in synthetic antiferromagnets, *Appl. Phys. Lett.* **118**, 112405 (2021).
- [36] D. A. Bozhko, H. Yu. Musiienko-Shmarova, V. S. Tiberkevich, A. N. Slavin, I. I. Syvorotka, B. Hillebrands, and A. A. Serga, Unconventional spin currents in magnetic films, *Phys. Rev. Res.* **2**, 023324 (2020).